Chemical and magnetic structure of uranium/gadolinium multilayers studied by transmission electron microscopy, neutron scattering, and x-ray reflectivity

R. Springell,[1,2,*] S. Langridge,[3,†] A. Wildes,[4] S. B. Wilkins,[5] C. Sanchez-Hanke,[5] K. T. Moore,[6] M. T. Butterfield,[6] J. Chivall,[2] R. C. C. Ward,[7] M. R. Wells,[7] and G. H. Lander[8]

[1]*European Synchrotron Radiation Facility, BP 220, F-38043 Grenoble Cedex, France*

[2]*Department of Physics and Astronomy, University College London, London WC1E 6BT, United Kingdom*

[3]*ISIS, Rutherford Appleton Laboratory, Harwell Science and Innovation Campus, Oxon OX11 0QX, United Kingdom*

[4]*Institut Laue-Langevin, BP 156, 38042 Grenoble Cedex 9, France*

[5]*Department of Condensed Matter Physics and Materials Science, Brookhaven National Laboratory, Upton, New York 11973-5000, USA*

[6]*Lawrence Livermore National Laboratory, Livermore, California 94551, USA*

[7]*Clarendon Laboratory, University of Oxford, Oxford, Oxon OX1 3PU, United Kingdom*

[8]*European Commission, JRC, Institute for Transuranium Elements, Postfach 2340, 76125 Karlsruhe, Germany*

(Received 12 January 2010; revised manuscript received 26 February 2010; published 29 April 2010)

We present a multitechnique approach to study the detailed chemical and magnetic structure of uranium/gadolinium multilayers. At low temperature the saturation magnetization is found to be ~60% of that of bulk gadolinium. We address this problem, which is found in many other multilayers and suggest a model that may have wider applications. transmission electron microscopy images indicate a microstructure, consistent with a columnar growth of Gd with crystallites of the order $20 \rightarrow 100$ Å. Off-specular neutron scattering is most strongly visible at saturation field, indicating that Gd moments are not aligned with the applied field. X-ray resonant magnetic scattering provides proof of coupled in-plane length scales for both the structural and the magnetic roughness. A detailed x-ray scattering study of both the specular and off-specular reflectivities has been used to investigate the in-plane structure of the multilayers. We calculate the roughness and transverse correlation cut-off length, $\xi_x = 120 \pm 30$ Å, and present a simple model to determine an average column size of 27 ± 6 Å and a reduction in the magnetic saturation of ~40%.

DOI: 10.1103/PhysRevB.81.134434 PACS number(s): 75.70.Cn, 78.70.Ck

I. INTRODUCTION

The determination of the physical properties of buried nanoscale layers and interfaces remains an important challenge in solid-state physics. The study of such systems is particularly appealing given the emergence of new physics and their technological relevance in areas such as data storage[1] and spintronics.[2] Clearly it is of paramount importance to possess an understanding of the magnetic structure given that much of the functionality of these systems resides within nanometers of the interface due to effects such as proximity and spin accumulation.[3–5] Increasingly, electronic reorganization at interfaces is leading to the observation of novel phenomena of potential importance for spintronic junction devices as has recently been demonstrated at the interface between two insulating perovskites.[6] Of comparable importance is the magnetic structure within the plane of the sample, which may not be homogeneous due to magnetic domains, grain boundaries, phase separation, etc. The logical conclusion is that a true three-dimensional (3D) understanding of the magnetic structure is required. It is in this respect that scattering techniques[7] have unique advantages to extract quantitative 3D information from buried structures complementing surface sensitive techniques such as microscopy. In this work we combine real and reciprocal space data to describe both the structure and magnetism of an inhomogeneous magnetic system in three dimensions.

With respect to changes in the saturation magnetization we shall confine our attention to systems involving gadolinium. There are good reasons for this; first, the Gd atoms in Gd metal can be considered as localized with seven $4f$ electrons with reasonably small anisotropy,[8,9] second, the moment is large $\sim 7.6 \mu_B$ and variations from this can be readily detected.

Many different systems involving Gd have been studied but in most cases the moments were not systematically determined. For example, there is extensive literature on the Fe/Gd system[10–15] but here the individual moments are difficult to determine although the strong polarizing field of the ferromagnetic Fe moments is assumed to align almost the full Gd moment.

A particularly informative series of experiments concerns off-specular x-ray resonant magnetic scattering. Whereas the specular scattering determines the roughness in the growth direction of the multilayer, and is routinely used, off-specular scattering is more complex, but gives information about the roughness in the transverse (i.e., in-plane) direction. Such a technique was applied to the Fe/Gd multilayers with the unexpected result that the charge roughness had a shorter transverse correlation length than the corresponding charge-magnetic correlation length.[14,15] As we shall see, in our present study we draw heavily on this type of analysis and also on an earlier work illustrating the methodology of determining charge correlation length cutoffs in the transverse direction in Mo/Si multilayers.[16]

Other examples are W/Gd and Mo/Gd. In using Si as a substrate for W/Gd the authors found saturation magnetizations close to the bulk values[17] whereas considerable reductions in these values were determined for Mo/Gd multilayers on glass substrates.[18] The difference between these two re-

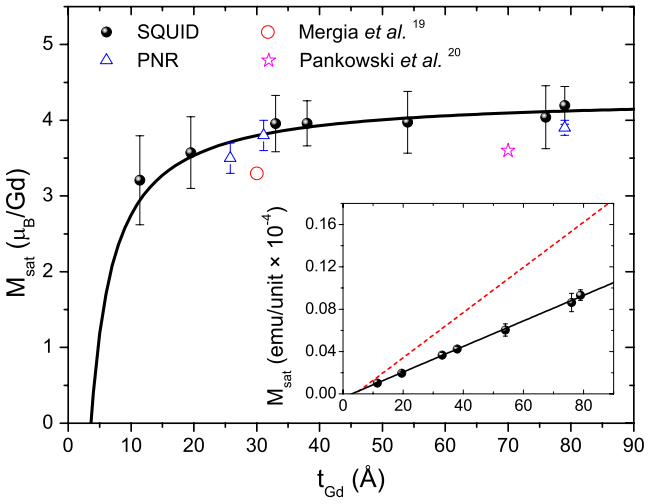

FIG. 1. (Color online) The magnetic moment per Gd atom is shown as a function of Gd thickness for a series of U/Gd multilayers with a uranium layer thickness of ~25 Å. The filled circles are data determined from SQUID magnetometry and the triangles, PNR. The solid line is a linear fit to the absolute saturation magnetization (shown in the inset), converted into units of μ_B/atom. The inset shows the saturation magnetization in units of emu/unit and a straight line fit to these data (emu/unit represents the absolute moment, scaled by the area of the sample and number of bilayer repeats). The dashed red line represents the expected values for the full moment of ~7.6μ_B. These data are adapted from Springell *et al.* (Ref. 23). Selected data from Gd/V and Gd/Cr multilayers are shown for comparison, adapted from Pankowski *et al.* (Ref. 19) and Mergia *et al.* (Ref. 20), respectively.

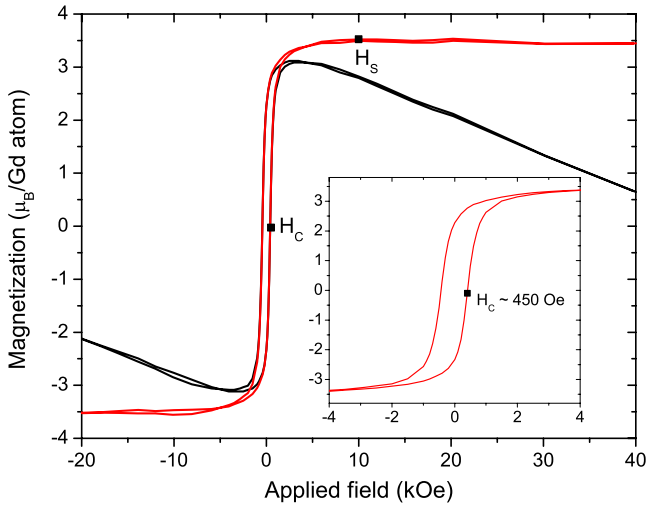

FIG. 2. (Color online) An example of the low-temperature magnetization behavior of a U/Gd multilayer with a Gd-layer thickness, t_{Gd}~50 Å. The black line shows the raw data, converted to values of μ_B/Gd and the red line is the data corrected for the linear dependence at high field, dominated by the diamagnetic response of the sapphire substrate. The inset shows the low field data. The coercive field, H_C, and the saturation field, H_S, are indicated on the graphs.

sults is unexpected as W and Mo are isostructural. In both cases the bcc transition metal (W or Mo) were textured (110) whereas the hcp Gd was predominantly textured *c* axis (0002). Gd/V (Ref. 19) and Gd/Cr (Ref. 20) multilayers have also been reported to exhibit significantly reduced saturation magnetizations and these are highlighted in Fig. 1. A common suggestion is that this reduction is an interfacial effect, however, our results indicate that this is not the case and that a great deal remains to be understood on this issue.

The present work originates from our research program, investigating the rich physics in the properties of the actinide metals[21] in reduced dimensions. Specifically, our interest in using uranium in multilayers is to study the interplay of 5*f* electrons and neighboring ferromagnetic elements with 3*d* and 4*f* electrons.[22–24] One striking result occurred in the U/Gd multilayers, in which the Gd ferromagnetic saturation was reduced by about 40% from its bulk value.

The variation in the saturation magnetization, shown in Fig. 1 exhibits two distinctive features: the first is the increase in M_{sat} from close to zero at a thickness of t_{Gd}=5 Å to ~3.5μ_B at t_{Gd}=20 Å. This implies a so-called "dead" layer thickness of approx. 5 Å, likely caused by intermixing of the U and Gd atoms. The second is that at the largest thicknesses the saturation moment still only attains a value of ~4.3μ_B, a reduction of ~40% from the bulk value of 7.6μ_B. This implies that the mechanism responsible for this large reduction in magnetization is not simply an interfacial effect, i.e., a magnetic dead layer, nor is it due to interfacial strain. This effect persists through the whole of the Gd layer thickness. The insert of Fig. 1 shows the absolute saturation magnetization, scaled to the number of layers and area of sample. The dashed red line shows the expected magnetization for Gd layers with the bulk moment values.

The low-temperature magnetization behavior should provide a clue as to why the saturation values are so low. Figure 2 presents an example field-dependent measurement of the magnetization for a U/Gd multilayer with t_{Gd}~50 Å, taken using an MPMS-7 superconducting quantum interference device (SQUID) magnetometer. Values for the coercive field, H_C, and the saturation field, H_S, are indicated in Fig. 2 and the insert, which shows the low field dependence. The difficulty encountered in an analysis of the high field magnetization is the dominant diamagnetic contribution from the sapphire substrate. This is a common problem in the study of multilayers, which must be grown on relatively thick substrate materials.

The present paper addresses these issues by using a combination of characterization methods. A cross-sectional transmission electron microscopy (TEM) study provides some insight into the microstructure of the U and Gd layers. The average in-plane structure is then characterized in detail by off-specular x-ray reflectivity, which is then used in combination with both off-specular-polarized neutron reflectivity (PNR) and diffuse x-ray resonant magnetic reflectivity (XRMR) to probe the magnetism of the Gd layers. The end product of this report is a simple model, supported by a number of experimental results, for the reduction in saturation magnetization.

II. SAMPLE FABRICATION AND PROPERTIES

The samples were prepared in the Clarendon Laboratory, University of Oxford, by dc magnetron sputtering in a UHV

load-locked growth chamber, operating at a base pressure of 5×10^{-10} mbar. The multilayers were grown on 50-Å-thick niobium buffer layers deposited onto single-crystal sapphire plates. The multilayers were sputtered at a growth rate of ~1 Å/s in an argon atmosphere of 5×10^{-3} mbar. The samples were protected from oxidation by a 50-Å Nb capping layer.

In most sputtered Gd films there is a tendency for the Gd layers to show strongly preferred orientation with the *c* axis along the growth direction and the same is found in our U/Gd multilayers.[22] Surprisingly, the uranium also develops an hcp structure, which is not found in the bulk,[22,25] but the crystallite sizes are small with a preferred orientation of (0002). The magnetic moment on the U $5f$ states[24] is $\sim0.02\mu_B$ and is negligible when discussing the reduction in the multilayer magnetization due to effects within the Gd layers.

In a bulk sample the moments are close to the *c* axis but in a thin film the shape anisotropy tends to align the moments in the plane of the film. Recent experiments[26] have shown that for a molecular-beam epitaxy film of Gd of 60 Å, the moments have their full value and lie in the plane of the film. Therefore, the above reference[27] sets a benchmark and we can conclude that the observed reduced saturation magnetization parallel to the in-plane applied field is not caused by the rotation of the moment out of the plane and toward the *c* axis in thin layers.

III. CROSS-SECTIONAL TEM

Cross-sectional TEM was performed on a sample of $[U_{50}/Gd_{50}]_{20}$. The TEM samples were prepared via focused ion-beam milling, where an electron-transparent slab was cut and extracted.

The $[U_{50}/Gd_{50}]_{20}$ multilayer is shown in Fig. 3, where (a) is a lower magnification and (b) is a high-resolution image showing the atomic lattice. Analytical TEM, such as electron energy-loss spectroscopy and energy-filtered imaging,[28] is not needed for two metals with highly divergent atomic numbers since mass contract due to electron scattering allows clear imaging of each chemical species.[29] In these images the Gd and U can be easily distinguished by mass contrast. Using this to our advantage, the degree of interdiffusion between U and Gd at the interfaces can be discerned. Based on reflectivity results reported earlier[22] a roughness of ~9 Å was expected and this length is consistent with the presently observed interdiffusion and structural roughness.

The crystal quality proved to be widely divergent between Gd and U layers. The Gd layers exhibit well-defined crystallinity, as seen by the lattice fringes in Fig. 3(b). On the other hand, the U layers show little or no lattice contrast, suggesting either very small crystallinity or an amorphous microstructure. In fact, the results of high-angle x-ray diffraction[22] show that both the U and Gd have a strongly preferred hexagonal microstructure with the *c* axis along the growth direction. Clearly, the microstructure in the hcp-U layers has small crystallites. Moreover, since no in-plane reflections have ever been observed with x rays in any U/Gd multilayer, this implies that there is no in-plane coherence. This is consistent with a detailed examination of Fig. 3(b). As discussed by Springell *et al.*,[22] the growth of the U/Gd multilayers has much in common with a poor superlattice, but the exact coherence necessary for such a superlattice is missing.

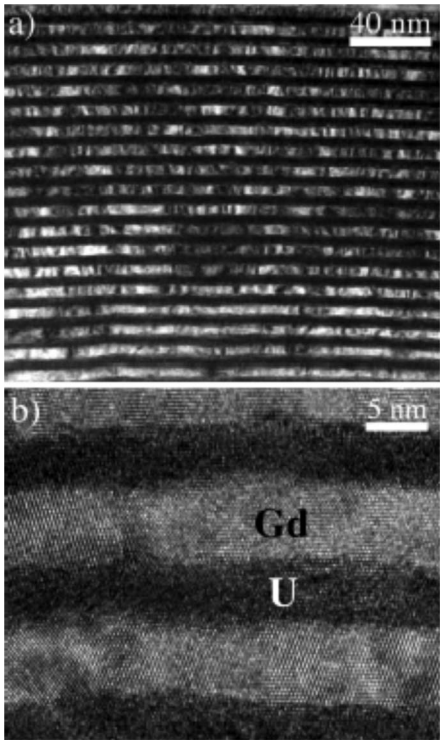

FIG. 3. TEM images of a $[U_{50}/Gd_{50}]_{20}$ multilayer (subscripts represent the layer thicknesses in Å and the number of bilayer repeats, respectively). The mass contrast between the U and Gd can be easily distinguished; the lighter Gd atoms scatter the electron beam less than the U atoms and thus appear brighter. The U and Gd layers are labeled in the high-resolution image (b); (a) shows a lower resolution. The scales are highlighted on the images.

An important aspect is the dimension of the crystallites in the Gd layers. One can observe from Figs. 3(a) and 3(b) that most crystal grains extend across the entire Gd layer thickness so that they may correctly be described as "columns" within the Gd layers. Indeed, this type of microstructure is often seen in metallic multilayers due to growth processes and interfacial strains. In terms of the lateral extent (D), there is clearly a large range, some appear at least twice the height, whereas others are relatively thin. A general comment would be that the columns appear to have a width between $0.4<D<2$ times the height, i.e., $20<D<100$ Å.

IV. X-RAY REFLECTIVITY

X-ray reflectivity, or low-angle x-ray diffraction, has become the ubiquitous characterization technique for thin films and multilayers. The most common, and easily interpretable geometry, is the so-called longitudinal or specular geometry. In this condition, the incoming x-ray beam probes the variation in electron density perpendicular to the plane of the multilayer surface, in the q_z direction. From measurements of this type it is possible to gain information on the layer thick-

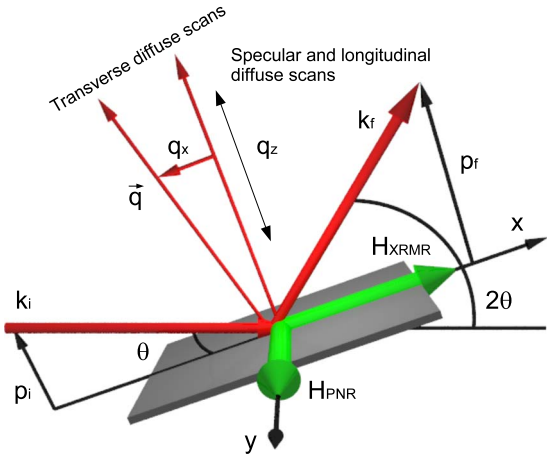

FIG. 4. (Color online) Schematic representation of reflectivity scans in reciprocal space. Measurements in a longitudinal geometry probe the electron density in the q_z direction; diffuse scans are off-specular at fixed positions of q_x, and specular scans satisfy the condition $q_x=0$. Measurements of the diffuse scattering in the transverse geometry, commonly termed rocking curves, are scans in q_x at approximately fixed q_z. k_i and k_f are the initial and final wave vectors, respectively, and their projection onto the axis normal to the sample surface is denoted by p_i and p_f, used for discussions in Sec. V. Applied magnetic fields parallel (H_{XRMR}) and perpendicular to the scattering plane (H_{PNR}) are represented by green arrows along the x and y axes, respectively; these are used to describe experimental conditions in Secs. V and VI.

nesses, densities, and interlayer widths. Here we have used the term "interlayer width" to describe what is commonly termed the roughness, since a structural roughness [root mean squared (rms) deviation in average layer height] is indistinguishable from diffusion of one species into another, a process which occurs on the atomic scale, even in systems often thought to be immiscible. Considering the behavior of the magnetization and the TEM data presented in the previous sections, it is clear that knowledge of the in-plane structure in these U/Gd multilayers is important. In this case, it is necessary to probe the electron density away from the surface normal, in the q_x direction, employing the off-specular x-ray reflectivity technique. Figure 4 shows a schematic reciprocal space diagram summarizing the directions probed in the most common scans carried out in reflectivity measurements.

In magnetic multilayers, it is the interfacial properties that most often dominate the overall characteristics. However, in our case we are concerned with identifying features that pervade through the whole thickness of the magnetic layers. Measuring the transverse diffuse scattering allows a separation of structural roughness and interfacial diffusion, determination of characteristic in-plane correlation lengths, and of the replication of roughness from one bilayer to the next; the vertical correlation length.

The experimental data were measured on a Philips reflectometer at Oxford, using a Cu $K\alpha$ tube source with a wavelength of 1.54 Å. Because the peak in diffuse scattering also occurs at the specular condition, it is necessary to correct for this effect in order to correctly model the specular reflectivity it is necessary to correct for this effect in order to correctly model the specular reflectivity. Data were collected in a longitudinal geometry just off of the specular ridge, at fixed q_x, and in the specular condition, $q_x=0$. The former was subtracted from the latter to yield the true specular reflectivity. We have used the GENX computer program, developed by Björk and Anderssen,[30] which uses the differential evolution algorithm to fit calculated reflectivities to experimental data, and is especially useful at avoiding local minima, a common problem when fitting reflectivity curves. The specular reflectivity was simulated using the Parratt recursion method of calculating reflected and transmitted wave fields.[31] The variation in electron density at the U/Gd interface was modeled as a Gaussian distribution,[32,33] combining both interdiffusion and roughness effects.

The free parameters included the bilayer thickness, determined precisely by the positions of the Bragg peaks, the gadolinium layer thickness, t_{Gd}, and therefore the uranium layer thickness, t_{U}, the respective roughnesses, σ_{Gd} and σ_{U}, the layer densities, and the corresponding parameters describing the Nb buffer, capping layer and the Nb oxide layer. This is standard procedure for the characterization of multilayers.

The use of the distorted-wave Born approximation (DWBA) formalism in the study of thin layers was refined by Sinha *et al.*[34] and then extended to the investigation of interface morphology in multilayered heterostructures.[35–44] A variety of layer topologies, including terraced,[45] stepped,[45] and fractal,[36] can be treated in these calculations. In our case, the fractal approach models our data well. We have used a fractal-type correlation function within the GENX program, which describes the height-height correlation of the layer surfaces, ξ_x (the lateral correlation length cutoff), the degree of partial correlation from one interface to the next; the vertical correlation length,[33,46] ξ_z, and the jaggedness of the surface; as defined by the so-called Hurst parameter, H, which takes values between 0 and 1. The surface fractal dimension, $D=3-H$ so that small values of H describe a very jagged surface and values of H approaching 1 have smoothly varying height distributions.

For a surface that can be described as self-affine or fractal in nature[47–50] the self-correlation function can be written as

$$C(\vec{\mathbf{r}}) = \sigma_i^2 e^{-(\vec{\mathbf{r}}/\xi_x)^{2H}}. \quad (1)$$

In this case σ_i represents the rms roughness of the ith layer. Including the partial correlation of the roughness from one layer to the next yields a correlation function

$$C_{i,j}(\vec{\mathbf{r}}) = \sigma_i \sigma_j e^{-(\vec{\mathbf{r}}/\xi_x)^{2H}} e^{-|\bar{z}_i - \bar{z}_j|/\xi_z}. \quad (2)$$

$\bar{z}_i$ and $\bar{z}_j$ represent the mean heights of the ith and jth layers, respectively. This correlation function relies on the central assumption that the differences in height from one point in the surface to another are distributed as a Gaussian random variable.

In a transverse diffuse scan the intensity measured at the detector position, $I(\vec{q})$, normalized to the incident flux, I_0, is a sum of contributions from the specular and diffuse scattering, which can be written as[15,16]

$$I(\vec{q})/I_0 = |\tilde{R}(q_z)|^2 \delta(\vec{q}_{xy}) + \frac{1}{l_x \times l_y} \int \left(\frac{d\sigma}{d\Omega}\right)_{diff} d\Omega. \quad (3)$$

The first term on the right of Eq. (3) represents the specular reflectivity and the second defines the diffuse scattering cross section, integrated over a solid angle d for an x-ray beam cross section with dimensions l_x and l_y. For the case where $q_z\sigma \ll 1$, the diffuse scattering yields the Fourier transform of the correlation function. The correlation function is the only term in the diffuse cross section that contains the correlated roughness explicitly, so it is important to probe the off-specular scattering in order to separate this from the total interfacial width.

In our case, we have measured the diffuse scattering from a $[U_{50}/Gd_{50}]_{20}$ sample. Transverse scans at five selected positions in q_z, labeled A–E are shown in Fig. 5. These correspond to the first two Bragg minima (A and C) and the first three Bragg peaks (B, D, and E). Figure 5 shows the experimental data as open black circles and the overall calculations are shown as blue solid lines. These are composed of contributions from the specular, modeled as a Gaussian, a Lorentzian contribution, narrow in q_z, due to crystal mosaicity, and the diffuse scattering determined by the DWBA formalism, shown as the solid red lines and as the inset in panel (b) of Fig. 5. Panel (a) displays the specular and diffuse measurements together with the projection of the extent of the diffuse scattering onto the (q_x, q_z) plane.

Table I summarizes the relative U and Gd layer thicknesses, roughnesses, correlation lengths, and Hurst parameter, determined from fits to the specular and diffuse scattering data, shown in Fig. 5. In order to determine a confidence level on the fitted parameters for the diffuse scattering, the intensity at the third Bragg peak position was calculated, varying the vertical correlation length (ξ_z), the Hurst parameter (H), and the lateral correlation length cutoff (ξ_x). These are shown in Fig. 6, displayed as three panels, respectively. It is then possible to assign tolerances on the fitted parameters and these are quoted in Table I.

In order to model the magnetic properties, in this case to determine the effect of the nanocrystallinity on the reduced saturation moment, we approached the problem by measuring off-specular polarized neutron reflectivity and soft x-ray resonant magnetic reflectivity at the Gd M_4 edge and these are described in detail in the following sections.

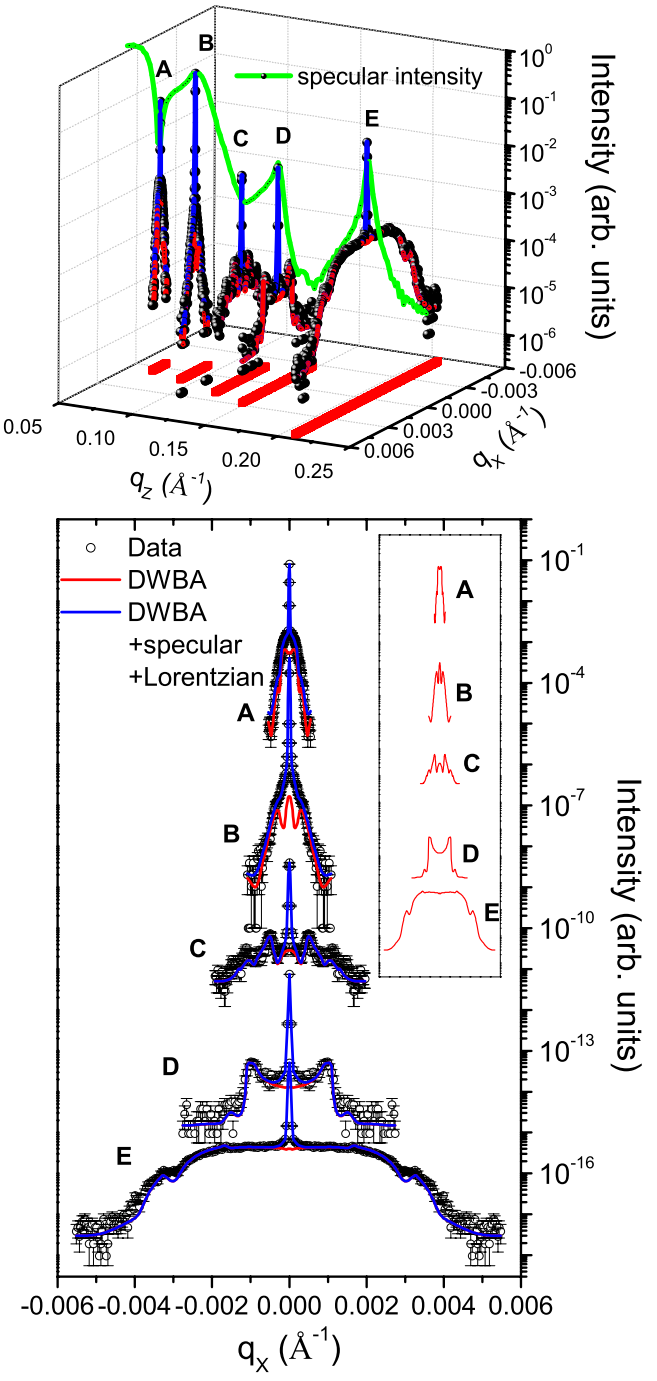

FIG. 5. (Color online) Contribution to off-specular scattering from DWBA (red) + specular and Lorentzian width (blue). Top panel (a) combines the transverse scans with specular reflectivity and shows the projection of q_x onto the q_x, q_z plane. A–E are the positions in q_z along the specular ridge at which transverse scans were made in q_x; A is at 0.067, B 0.090, C 0.121, D 0.150, and E is at 0.210 Å^{-1}. Bottom panel (b) shows transverse scans, scaled for clarity. Inset shows the contributions from diffuse scattering only, modeled using DWBA with GENX package.

V. OFF-SPECULAR-POLARIZED NEUTRON REFLECTIVITY

Neutron and x-ray reflectivity are complementary techniques; x-ray photons of wavelength λ, probe the electron density; neutrons of wavelength $\lambda = h/\sqrt{2mE}$, probe the neutron-scattering length density. In the same way as for x-rays, calculations of the specular neutron reflectivity yield the layer thickness, interlayer width, and density.[51]

Neutrons have one distinct advantage over x-rays in that their intrinsic spin couples directly to the magnetic induction of the sample. In fact, the magnetic potential that the neutron experiences in the sample is of comparable size to the neutron nuclear interaction. The potential involved in the neutron-sample interaction contains a term, V_m to describe the magnetic induction, where p is the magnetic scattering length and N is the atomic number density.

TABLE I. The fitted parameters of layer thickness and roughness for the U and Gd layers, respectively, the in-plane correlation length cutoff and the vertical correlation length. All values are given in Å. H is the dimensionless Hurst parameter.

Gadolinium layer thickness,	t_{Gd}	48 ± 1
Gadolinium structural roughness,	$\sigma_{c_{\mathrm{Gd}}}$	7 ± 1
Diffuse gadolinium layer,	$\sigma_{d_{\mathrm{Gd}}}$	1.5 ± 0.5
Uranium layer thickness,	t_U	47 ± 1
Uranium structural roughness,	σ_{c_U}	5 ± 1
Diffuse uranium layer,	σ_{d_U}	2.5 ± 0.5
In-plane correlation length cut-off,	ξ_x	120 ± 20
Vertical correlation length,	ξ_z	700 ± 200
Roughness exponent, Hurst parameter,	H	0.3 ± 0.05

$$V_m(z) = -\mu_N \cdot \mathbf{B}(z) = \frac{2\pi\hbar^2}{m} N p(z). \tag{4}$$

The experimental geometry is shown in Fig. 4, Sec. IV. The magnetic field (H_{PNR}) is applied perpendicular to the scattering plane, along an axis, x, parallel to the neutron-quantization axis. The total potential, V, is a sum of contributions from the nuclear (where b is the neutron nuclear-scattering length) and magnetic interactions. PNR takes advantage of this potential in two specific cases; that of nonspin-flip scattering and spin-flip scattering (SF). The former describes the situation where the incident and reflected neutron spin eigenstates are the same; it is measuring only the component of the magnetic induction parallel to the neutron spin, yielding a magnetic scattering length, $p_{\parallel}$, and potentials and reflectivities that can be represented as V_{++}, V_{--}, R_{++} (spin up), and R_{--} (spin down), respectively. SF scattering measures the component of the magnetization perpendicular to the neutron spin, within the plane of the sample, i.e., a magnetic scattering length, $p_{\perp}$. In this case the potentials and reflectivities can be labeled V_{+-}, V_{+-}, R_{+-}, and R_{-+}.

$$V_{++}^{--} = V_n \pm V_m = \frac{2\pi\hbar^2}{m} N(b \mp p_{\parallel}), \tag{5}$$

$$V_{-+}^{+-} = \frac{2\pi\hbar^2}{m} N(p_{\perp}). \tag{6}$$

The reflectivities of the neutron scattering from magnetic samples can be represented in a matrix form

$$\begin{pmatrix} R_{++} & R_{+-} \\ R_{-+} & R_{--} \end{pmatrix} \propto \begin{pmatrix} (b-p_{\parallel})^2 & p_{\perp}^2 \\ p_{\perp}^2 & (b+p_{\parallel})^2 \end{pmatrix}. \tag{7}$$

In the case that the polarization of the scattered beam is not analyzed, as in our case, the spin-up intensity $I^+ = R_{++} + R_{+-}$, and the spin-down intensity $I^- = R_{--} + R_{-+}$. The difference, $I^+ - I^-$ gives the quantity $4bp_{\parallel}$. Thus, the magnetic moments projected along the applied field direction are seen through their coherent interference with the nuclear scattering length, b.

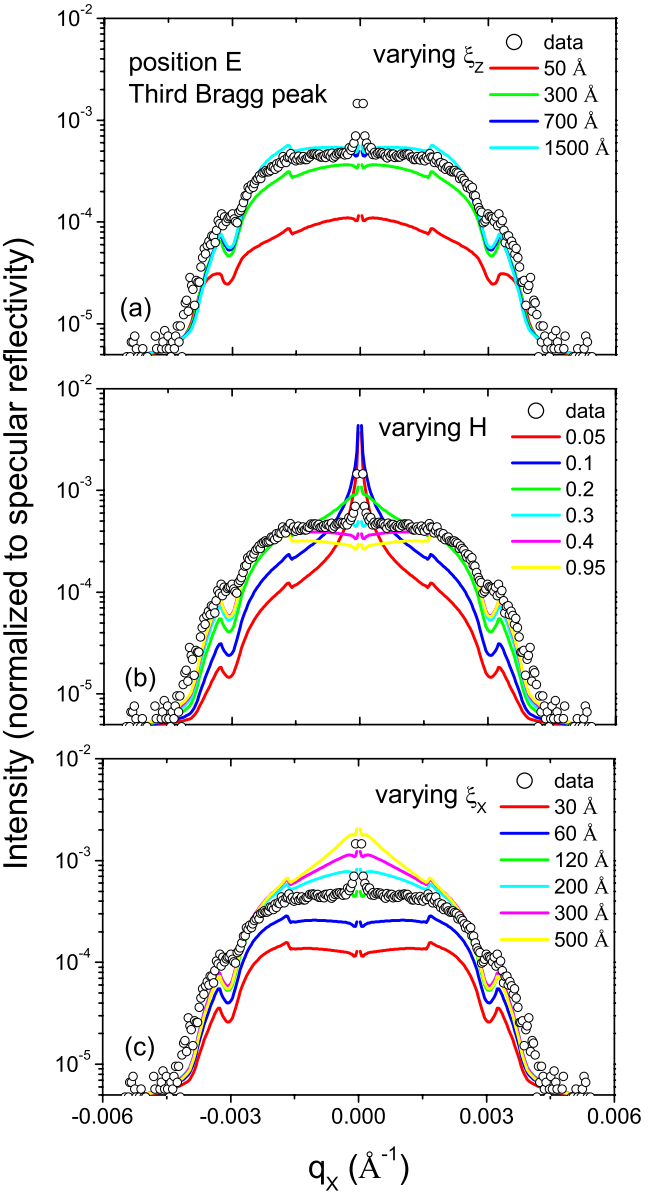

FIG. 6. (Color online) Figure showing the effects of varying the three variables in the modeling of the in-plane x-ray scattering. Panel (a) shows the influence of ξ_z, the vertical correlation length; panel (b), the influence of H, the Hurst parameter, which describes the jaggedness of the interface layer; and panel (c), the effect of ξ_x, the lateral correlation length cut-off.

Polarized neutron reflectivity in the specular condition from this system has been reported elsewhere.[23] However, diffuse scattering can be used to gain valuable information about the lateral landscape of the multilayer interfaces in much the same way as for x-rays and in this case we are now also sensitive to the magnetization profile. In the previous section we obtained a lateral correlation length cutoff of 120 Å, which describes features that are relatively small in real space and therefore extend to large lateral length scales in reciprocal space. There is a considerable difficulty in gleaning any quantitative conclusions from diffuse neutron reflectivity, since in order to probe structures that are large in q_x it is necessary to measure scattering around the highest

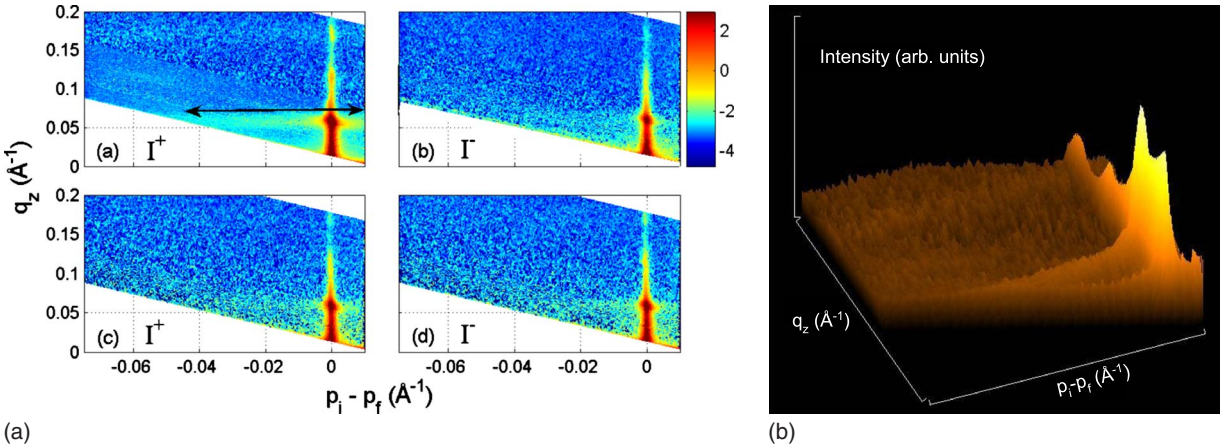

FIG. 7. (Color online) The left panels, (a)–(d) show the polarized neutron reflectivity as a function of q_z and $p_i - p_f$, measured at 5 K in monochromatic mode, with a neutron wavelength of 5.37 Å. (a) and (b) were measured in an applied magnetic field (10 kOe) for I^+ and I^- channels, respectively. (c) and (d) were measured at coercive field (0.72 kOe). The panel on the right-hand side shows a surface plot of the nuclear-magnetic diffuse scattering, visible about the first and third Bragg peaks at 5 K in a (10 kOe) applied field.

order Bragg peaks possible, i.e., at large values of q_z.

In order to optimize our chance of measuring diffuse scattering in the U/Gd system, we grew a $[U_{50}/Gd_{50}]_{50}$ sample on a large substrate, 20 mm × 24 mm. Our measurements were made on the D17 reflectometer at the ILL reactor source in Grenoble. The experiment was carried out in a horizontal scattering geometry using a monochromatic neutron beam of 5.37 Å. A magnetic field of up to 10 kOe could be applied in the plane of the sample, perpendicular to the propagation direction of the incident neutrons and parallel to their quantization axis. The maximum value of q_z at which adequate statistics were collected was about 0.2 Å^{-1}. Due to the small structural features present in the U/Gd multilayers, it was not possible to determine quantitatively any lateral length scales of the structure. However, an examination of the PNR as a function of field sheds light on behavior of the magnetic structure, i.e., observation of the magnetic roughness or domain scattering.[52]

Panels (a) and (b) of Fig. 7 show measurements of the diffuse scattering in a saturation field of 10 kOe; the I^+ and I^- channels, respectively. The lower panels, (c) and (d), present the scattering observable at coercive field. The coercive field was determined by carefully mapping the magnetization hysteresis of the sample until no splitting was observed between I^+ and I^- reflectivities in the specular condition. This position is labeled H_C in Fig. 2 and is within the error bars of the 0.72 kOe value determined in the neutron measurements due to the relatively coarse settings on the magnet.

The diffuse scattering is presented as a function of the wave-vector momentum transfer perpendicular to the plane of the film, q_z, and $(p_i - p_f)$, where p_i and p_f are the perpendicular projections of incoming and scattered neutron wave vectors, respectively. This method of displaying the data is useful for investigating the scattering at low q_z, which in a q_x representation would be much harder to distinguish from the intensity around the specular ridge. This is especially important in our case where the majority of the diffuse scattered intensity is centered around the first Bragg peak at 0.065 Å^{-1}, which has an extent in q_x of 3×10^{-4} Å^{-1} in the positive direction and 7×10^{-4} Å^{-1} in the negative, highlighted by the arrow in Fig. 7, panel (a).

The diffuse scattered intensity observed in Fig. 7 is unusual. The commonly observed situation in diffuse scattering from magnetic multilayers is that of an intense plane of scattering about the Bragg peak positions at the coercive field, with features observable that have lateral length scales on the order of microns. This is commonly attributed to scattering from domains.[53] The intensity then disappears at saturation field, since what remains is a single domain state. In Fig. 7, a small, but detectable diffuse scattered intensity can be observed around the first Bragg peak in both the I^+ and I^- channels at the coercive field. This is a weak and very broad feature, likely arising from correlated roughness from small structural features in the plane of the film, in a similar vein to that observed in the x-ray reflectivity measurements. At saturation field, labeled H_S in Fig. 2 and referring specifically to the ferromagnetic component of the Gd layer, a strong ridge of intensity is present in the I^+ channel only, panel (a); this is shown in more detail in the surface plot in the right-hand panel of Fig. 7. This can be understood in terms of the addition of scattered intensity to that from the correlated structural roughness in the I^+ channel, panel (a), and a subtraction in the I^- channel, panel (b). This can be interpreted as a magnetic roughness, which is of a similarly broad nature in reciprocal space to the structural picture and hence is due to small features in real space.

VI. DIFFUSE X-RAY RESONANT MAGNETIC REFLECTIVITY

By employing circularly polarized synchrotron radiation and applying a magnetic field at the sample position, the magnetic signal is detected as the difference in intensity of the elastic scattering when either the helicity of the incoming x rays or the magnetic field direction is reversed. The experimental geometry is shown in Fig. 4, including the magnetization direction, for a typical XRMR measurement. The scattering plane, defined by the incident and scattered wave

vectors (k_i and k_f at an angle θ to the y axis), is parallel to the yz plane, where the z axis is defined as perpendicular to the multilayer surface. The mathematical description of specular and diffuse x-ray resonant magnetic scattering, specifically in a reflectivity geometry have been discussed in detail elsewhere.[11,13–15,54–57] Here, we summarize some salient points.

For the case of ferromagnets, the charge and magnetic structure factors are

$$F_c = \sum (f_0 + f_c' + if_c'')e^{(i\vec{q}.r_j)}, \tag{8}$$

$$\mathbf{F_m} = \sum \hat{z}_j(f_m' + if_m'')e^{(i\vec{q}.r_j)}. \tag{9}$$

$f_0=Z$ is the atomic number, $\hat{z}_j$ is a unit vector in the direction of the magnetic moment on atom j, f_c' and f_c'' are the anomalous dispersion corrections to the charge scattering factors and f_m' and f_m'' are the resonant magnetic scattering factors. The experimentally determined quantity is the difference between the reflected intensities for right and left circularly polarized (RCP and LCP) x-rays, which can be obtained by reversing an external magnetic field or changing the helicity of the incoming beam. Since the intensity is proportional to the square of the amplitude, there are crossterms in the magnetic- and charge-dependent structure factors, which result in a magnetic-charge interference term that can be determined by the difference in helicity dependent intensities, I^+ and I^-

$$I^+ - I^- = -2(\hat{\mathbf{k}}_i + \hat{\mathbf{k}}_\mathbf{f} \cos 2\theta) \cdot (F_c'\mathbf{F_m'} + F_c''\mathbf{F_m''}). \tag{10}$$

Here, the charge structure factor and the resonant magnetic structure factor have been separated into their respective real and imaginary parts, which are real quantities for the case of centrosymmetric structures. The first term indicates that the magnetic charge interference is only sensitive to the magnetization component parallel to $\hat{\mathbf{k}}_\mathbf{i}+\hat{\mathbf{k}}_\mathbf{f}\cos 2\theta$ in the scattering plane. The interference between the charge and magnetic scattering, in an exact analogy with that observed in PNR as discussed in Sec. V.

The reflected intensity for multilayer samples was treated using the method described in Sec. IV. Recalling the equation for the refractive index and the scattering geometry displayed in Fig. 4, the refractive index for left and right helicity, circularly polarized x-rays becomes

$$n^\pm = 1 - \delta^\pm + i\beta^\pm, \tag{11}$$

where

$$\delta^\pm = \left(\frac{2\pi n_0 r_e}{k^2}\right)(f_0 + f_c' \mp f_m' \cos\theta \cos\phi) \tag{12}$$

and

$$\beta^\pm = \left(\frac{2\pi n_0 r_e}{k^2}\right)(f_c'' \mp f_m'' \cos\theta \cos\phi). \tag{13}$$

n_0 is the number of atoms per unit volume, r_e is the radius of the electron, θ is the angle between the incident x-ray beam and the sample in the scattering plane, and ϕ is the angle between the sample magnetization and the scattering plane. Both the charge and magnetic scattering factors show a strong energy dependence in the vicinity of an absorption edge, such that a fluorescence measurement is required for the case of right and left circularly polarized photons. The imaginary part of the charge scattering factor, f_c'' can be derived from the nonmagnetic absorption $(I^+ + I^-)/2$, whereas the magnetic scattering factor, f_m'' is related to the absorption coefficient, μ_m

$$\mu_m = -\left(\frac{8\pi n_0 r_e}{k}\right)(\hat{\mathbf{k}} \cdot \hat{\mathbf{z}})f_m'', \tag{14}$$

which can be probed in an x-ray magnetic circular dichroism (XMCD) measurement, $(I^+ - I^-)/2$. Circularly polarized x-rays are used in reflectivity measurements due to the tan 2θ factor present in the scattering of plane polarized x-rays.[58] In most experiments, flipping the helicity of the incoming x-rays is preferred to flipping the direction of the applied magnetic field since if the magnetic moments are not fully saturated they will not all reverse their direction when the field is reversed.

Given that we are concerned with the directions of the Gd magnetic moments in the plane of the film, we can make use of the XRMR technique in the off-specular geometry, treated within the same DWBA framework as for the laboratory-based x-ray diffuse scattering measurements. In order to probe the Gd magnetization, we used soft x-rays at the Gd M_4 and M_5 edges, which involve transitions from the $3d_{3/2}$ and $3d_{5/2}$ electronic core states to the unfilled valence-band $4f_{5/2}$ and $4f_{7/2}$ states, directly probing the $4f$ electrons responsible for the magnetism in gadolinium.

The data were collected at the X13A beamline of the National Synchrotron Light Source, Brookhaven National Laboratories. This beamline has been especially designed for reflectivity measurements, using x-rays with a 70% degree of circular polarization from an elliptical polarized wiggler source that can reverse the helicity at a frequency of 22 Hz. The same sample as that used for the earlier x-ray measurements ($[U_{50}/Gd_{50}]_{20}$) was mounted inside a two-circle vacuum compatible diffractometer at 10 K, where magnetic fields of up to 2 kOe could be applied at the sample position. A soft x-ray photodiode was used to detect the scattered x rays while the total electron yield (TEY) was simultaneously measured via the sample current. The TEY was measured across both Gd M_4 and M_5 edges, from 1175 to 1235 eV. In this way we were able to determine the maximum of the XMCD signal across the Gd M_5 edge (the intensity is greater than at the M_4), and then measure the diffuse magnetic scattering and the element specific hysteresis curve at this energy. For the case of the off-specular scattering, the difference signal between RCP and LCP x-rays was measured with the field applied parallel to the scattering plane and antiparallel to confirm the magnetic origin of the scattering.

Figure 8 shows a series of three panels: (a) presents the diffuse scattering data, measured at the third Bragg peak, labeled E in Fig. 5. The black open circles are the experimental data of the sum of the scattering from LCP and RCP x-rays and the blue open circles are the experimental data of

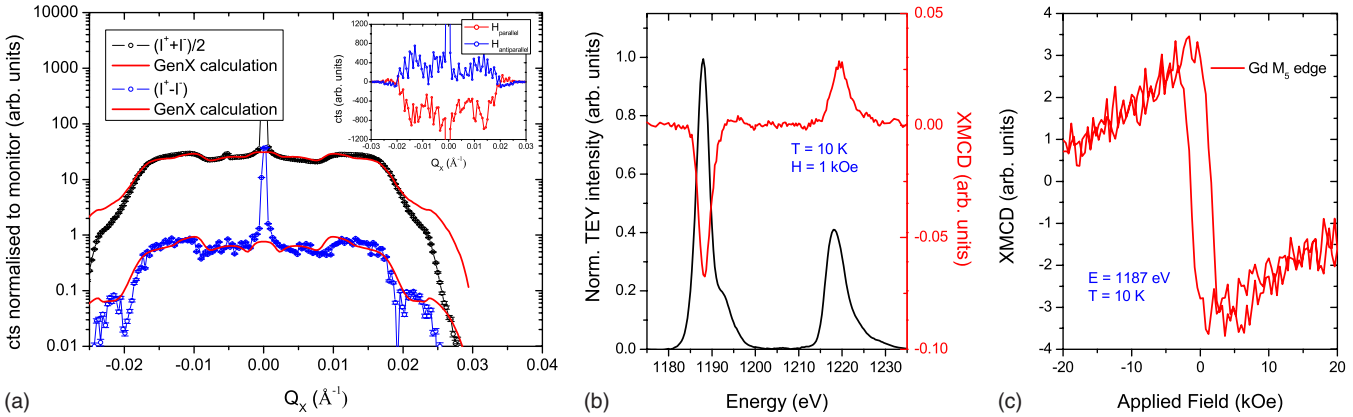

FIG. 8. (Color online) Panel (a) shows charge diffuse scattering (black) at the Gd M_5 edge and the magnetic diffuse scattering (blue) modeled using DWBA genx package (red). The inset shows the magnetic diffuse scattering with the magnetic field applied parallel to the beam direction (red) and antiparallel (blue). Panel (b) shows x-ray absorption near edge spectra and XMCD spectra measured at the Gd M_4 and M_5 edges, taken at 10 K and in an applied field of 1 kOe. (c) shows the hysteresis measured at 1187 eV (Gd M_5 edge) at 10 K.

the difference with the magnetic field applied parallel to the incident x-ray beam. The solid red lines are calculations. The inset shows the full reversal of the signal with the field applied parallel (blue open circles) and antiparallel (red open circles) to the scattering plane. (b) shows the Gd M_4 and M_5 edge TEY absorption spectra, at 10 K in an applied magnetic field of 1 kOe, labeled H_{XRMR} in Fig. 4. The red solid line is the XMCD signal, not corrected for saturation effects. The maximum of the (negative) XMCD signal at the Gd M_5 edge can be seen at 1187 eV, which was the energy used for the experiments shown in panels (a) and (c). (c) shows the element specific hysteresis curve measured at this energy.

The calculations of the diffuse scattering shown in Fig. 8, panel (a) were made using the DWBA framework with the GENX package,[30] used for the earlier Cu $K\alpha$ data presented in Sec. IV. The charge scattering factor was taken from the absorption data and the magnetic term was determined from the XMCD signal. The diffuse charge scattering could be modeled with the same parameters as those used for the experiments with Cu $K\alpha$ and shown in Fig. 5; vertical correlation length 700 Å, correlation length cutoff 120 Å and $H \sim 0.3$. For the calculation of the charge magnetic diffuse scattering, the exact same values could be used to model the data, i.e., the distribution of magnetic moments possesses the same in-plane characteristics as those of the underlying chemical structure. This is an important result in terms of trying to understand the mechanism for the magnetization behavior. It means that when determining the size of the crystallite dimensions we are also describing the magnetic features present.

VII. MODEL FOR REDUCTION IN MAGNETIZATION

We now possess several important pieces of information regarding the behavior of the gadolinium in the plane of the multilayer: (1) the SQUID magnetization shows a constant, reduction in saturation magnetization to $\sim 4.3 \mu_B$. (2) The TEM indicates that the Gd is present in small crystallites, between 25 and 100 Å in lateral dimension. (3) Calculations of the off-specular x-ray reflectivity indicate a lateral correlation length cutoff of ~120 Å for the structural roughness. (4) Off-specular PNR data suggest that unsaturated moments persist even at applied magnetic fields up to 10 kOe. (5) Diffuse XRMR can be calculated using the same parameters for both chemical and magnetic diffuse scattering, indicating that the in-plane structural features are of the same size as the magnetic ones.

In order to model the reduction in saturation magnetization, we start by making two important assumptions: first, that the magnetic moments at the crystallite boundaries are pinned, such that the perimeter of the columnlike structures do not contribute to the saturation magnetization, as determined by SQUID magnetometry. Second, that the symmetry of the crystallites possess the same hexagonal symmetry as the underlying Gd crystal structure.

Figure 9 shows a slice through the (x,y) plane of a single columnlike crystallite of hexagonal symmetry. The magnetic moments of the central atoms (red) are aligned with the applied field, **H**, whereas the outer moments are pinned at the crystallite boundary. The pinning is equally likely to occur in all in-plane directions so that when averaged throughout the multilayer, their contribution to the overall magnetization will be zero. It is then possible to calculate the likely reduc-

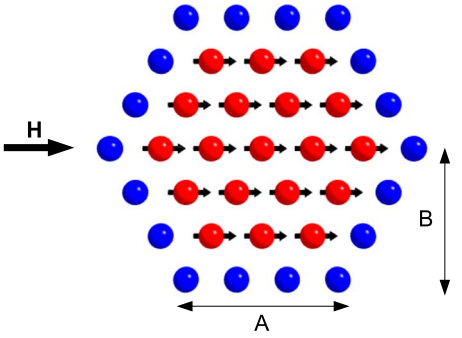

FIG. 9. (Color online) Diagram depicting Gd atoms (colored spheres) in a columnlike structure as viewed in the (x,y) plane. The moments of the central atoms (red) align with the applied magnetic field. The moments at the perimeter are pinned in random directions so that they make no contribution to the magnetization.

TABLE II. Summary of the expected reductions in saturation magnetization for crystallites of various lateral dimensions.

Total number of atoms	Atoms at the perimeter	Lateral dimension, D (Å)	Reduction in M_{sat} (%)
7	6	10.2	86
19	12	16.9	63
37	18	23.7	49
61	24	30.5	39
91	30	37.3	33
127	36	44.0	28
169	42	50.8	25

tion in the saturation magnetization as a function of lateral dimension, $D=(A+B)$; A is the side length of the hexagon and B is the distance from the center, normal to the side, see Fig. 9. Ad extremis, if the crystallites were extremely small, i.e., one atom across, then the reduction would be 100%, if the crystallites were microns in size then the pinning at column boundaries would have negligible effect on the observed saturation magnetization. Table II summarizes the expected reduction in M_{sat} for a given lateral size, D, for regular hexagonal dimensions, taking a_{Gd} to be close to the bulk value of 3.631 Å.

Clearly, the most important parameter to calculate is the average size of the columns, which has already been indicated to be between 20 and 100 Å from TEM measurements. The rms roughness determined from Cu $K\alpha$ diffuse reflectivity measurements is ~7 Å, which taking the lattice spacing, d, along the c-axis direction to be ~2.9 Å, is approximately $2d$. The variation in column heights is modeled as a Gaussian random variable, about an average layer thickness ($16d$). Figure 10 shows the expected Gaussian distribution of likely column heights, which can be determined using the rms value for the roughness, which is equivalent to the standard deviation. The solid red line shows the Gaussian line shape whose integral is unity. A histogram of probability versus column height is displayed since the column heights are taken to vary only in units of the lattice spacing, d.

A further simplification can also be applied: the in-plane structure is modeled as consisting of coaligned hexagonal crystallites of equal size. This allows for a determination of the average distance between crystallites of equal height for a given probability. For example, if the probability of having a column height, h, is 1/3 (highlighted as the red hexagons in the inset of Fig. 11) the average distance between these columns is $L=2\sqrt{3}B$. The variation of L as a function of the inverse of the probability is shown in Fig. 11; calculated points are represented by the black solid circles, the dashed red line shows a power-law function, describing this variation. We recognize the simplicity of this model. For example, the exact arrangement of the columns cannot be as shown as in Fig. 11, otherwise we would be able to observe off-specular Bragg points from the multilayer samples and this is not the case. However, the model serves as a general guide to calculate the average size of the columns and thus the reduction in the saturated magnetization.

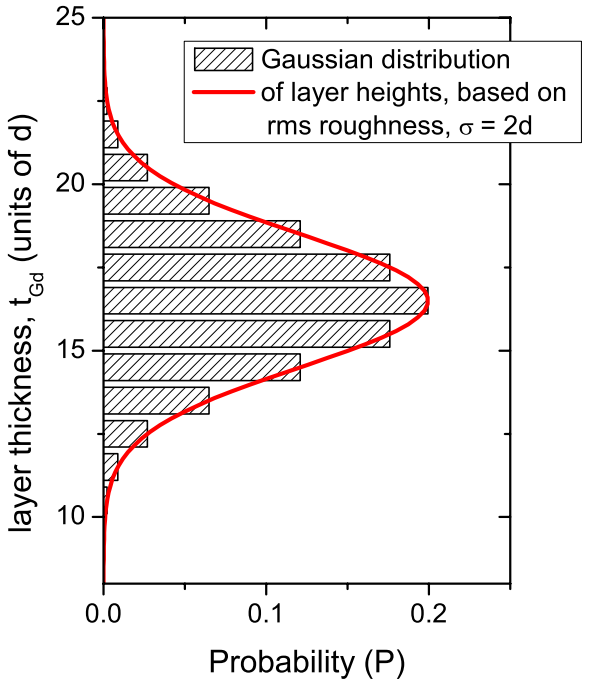

FIG. 10. (Color online) The figure shows a Gaussian distribution of layer thickness, t_{Gd}, and the corresponding probability. The average thickness of the layer is approx. $16d$, where d is the lattice spacing ($d\sim2.9$ Å). The rms roughness (equivalent to the standard deviation for a Gaussian distribution), $\sigma_c\sim2d$, determined from the calculations of the specular and diffuse reflectivities.

With this model we can determine an average separation between crystallites of equal height for the Gaussian distribution of column heights pictured in Fig. 10. Further, a sum of all possible separations, weighted by the probability for a specific crystallite height, gives the average column separation in units of D. For the case of an rms roughness, $\sigma_c\sim2d$, the average separation $L=4.51D$. The x-ray diffuse x-ray reflectivity measurements yielded $\xi_x\sim120$ Å. From these we extract $D=120/4.51=27$ Å. Table II gives a sum-

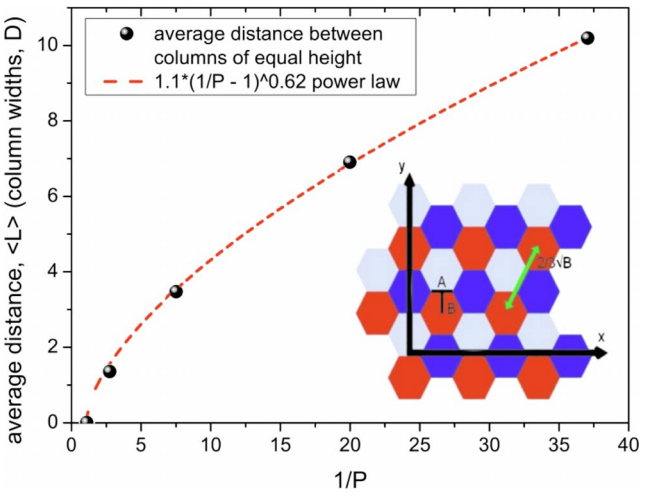

FIG. 11. (Color online) Plot of the average height-height correlation distance, L (units of column width, D), as a function of the inverse of the probability, $1/P$.

mary of the reductions in saturation magnetization expected for various crystallite sizes. For $D \sim 27$ Å the reduction is ~40%; a value close to that observed in SQUID magnetometry measurements (see Fig. 1).

VIII. DISCUSSION

The results of the present paper show that the reduction in the Gd magnetization is likely due to pinning of the moments at the perimeters of single-crystal-like columns within the Gd layers. The columnar growth is observed directly in cross-sectional TEM measurements (Fig. 3). Together with the observed structural roughness of the Gd layers, $\sigma_{c_{\mathrm{Gd}}}$ (Table I) of ~7 Å (from the specular reflectivity), and ξ_x ~120 Å (from the off-specular diffuse charge scattering as shown in Figs. 5 and 6), we can deduce a width for the columns of about 27 Å (Fig. 11).

In addressing the magnetism, we first note that (Fig. 7) the off-specular neutron signal is strongest at the saturation field and in the I^+ channel. Since the lateral correlation length cutoff, ξ_x, is relatively small (120 Å), to get a reliable result one has to have data to large q_x, and this is impossible to achieve with neutrons as the available intensity at the third Bragg peak is too small. Instead we have used off-specular diffuse x-ray resonant magnetic reflectivity at the Gd M_5 edge (Fig. 8) to show that the magnetic contribution can be fit with the same ξ_x as the charge. This leads to a simple idea that the moments are pinned at the perimeters of the columns (Fig. 9) and that the reduction in the magnetic moment from the bulk value of Gd depends on the size of the columns (Table II). The effect persists through the whole Gd layer and cannot be an interfacial effect, as noted earlier.[23]

A number of further questions are posed by this model. First, given that the Gd structural roughness increases with increased Gd thickness,[22] what is the likely change in the column distributions? Second, we observed that with increasing U thickness the Gd moments were even further reduced to below $3\mu_B$, i.e., ~60% reduction from the bulk value.[23]

The first point is relatively easy to understand. As the roughness increases, the spread of column heights does as well so the average distance between similar columns must also increase. This scaling relation ensures that column sizes remain about the same, assuring a constant reduction in moment as a function of Gd thickness, as shown in Fig. 1. The second point is more difficult. According to the simple model, a decreased magnetization implies a decrease in the average column size. Unfortunately, we have not performed enough in-depth studies of different U/Gd multilayers to be able to address this point but it does show the subtle interaction between the growth conditions and the magnetization of the ferromagnetic Gd. For example, the hcp nature of the growth in the U layers, even though of small crystallites, probably has an effect on the growth of the columns within the Gd layers.

In comparison to other work, we note that in the Fe/Gd multilayers much longer magnetic lateral correlation length cutoffs were found, extending to ~1000 Å, whereas the charge value[15] was 240 Å. In an earlier study of U/Fe multilayers,[59] we found a structural lateral correlation length of 200 Å, and a magnetic of ~3600 Å; clearly rather similar to the results in Fe/Gd. No TEM has been reported on either of these systems, but we might expect an absence of columnar growth in both cases. Of course, there are important differences between these two systems involving Fe and the one studied here, U/Gd. In U/Fe multilayers, for example, the bulk value of the Fe magnetic moment are found in the center of the Fe layers but dead layers are found at the interfaces. The interfaces in U/Fe are extremely complex[60,61] and we would not expect any similarities between that and the present U/Gd systems.

A number of other systems have been studied but mainly involving transition-metal systems. One of interest is that on CoFe/Cu thin films.[62] In this work, they investigated trilayers, which were manufactured with different chemical roughness (from ~600 to 1200 Å), and a relationship found between the magnetic and chemical lateral correlation lengths such that the magnetic correlation length is longer, by about 500 Å, than the chemical one. Although the numerical values are different, in studying Co films and Co/Cu/Co sandwiches, Mackay *et al.*[56] found lateral correlation lengths of ~500 Å, but again they find, in general, that the magnetic lateral correlation length is longer than the chemical one. In these systems, there is likely a different growth mechanism than the one we have found in U/Gd multilayers.

In conclusion, we have presented a comprehensive and detailed investigation of the structural and magnetic behavior of a very specific multilayer system, but it is our hope that this general approach can be used in other studies of multilayer systems. Reduction in the saturation magnetic moment and other effects caused by granular in-plane structures in thin-film systems could have wider implications in other more commercial combinations of elements. The ability to construct such idealized models, which are within suitable confidence levels of experimental results and backed up by several complementary techniques, could pave the way for the development of other real-space models coupled to reciprocal space probes.

ACKNOWLEDGMENTS

J. Chivall would like to thank the EPSRC, U.K. Our group would like to thank the Atomic Weapons Establishment (AWE), U.K. for providing the depleted U target and ITU, JRC Karlsruhe for financial assistance. We also owe our gratitude to R. A. Cowley, W. G. Stirling, and S. W. Zochowski for useful discussions.

*ross.springell@ucl.ac.uk
†http://www.isis.rl.ac.uk/

[1] C. Chappert, A. Fert, and F. Nguyen Van Dau, Nature Mater. **6**, 813 (2007).
[2] I. Žutić, J. Fabian, and S. Das Sarma, Rev. Mod. Phys. **76**, 323 (2004).
[3] M. Johnson and R. H. Silsbee, Phys. Rev. Lett. **55**, 1790 (1985).
[4] F. Jedema, A. Filip, and B. van Wees, Nature (London) **410**, 345 (2001).
[5] A. Brataas, Y. Tserkovnyak, G. E. W. Bauer, and B. I. Halperin, Phys. Rev. B **66**, 060404(R) (2002).
[6] A. A. Brinkman, M. Huijben, M. van Zalk, J. Huijben, U. Zeitler, J. C. Maan, W. G. van der Wiel, G. Rijnders, D. H. A. Blank, and H. Hilgenkamp, Nature Mater. **6**, 493 (2007).
[7] C. Marrows, L. Chapon, and S. Langridge, Mater. Today **12**, 70 (2009).
[8] J. W. Cable and E. O. Wollan, Phys. Rev. **165**, 733 (1968).
[9] M. Colarieti-Tosti, S. I. Simak, R. Ahuja, L. Nordström, O. Eriksson, D. Åberg, S. Edvardsson, and M. S. S. Brooks, Phys. Rev. Lett. **91**, 157201 (2003).
[10] J. Landes, C. Sauer, B. Kabius, and W. Zinn, Phys. Rev. B **44**, 8342 (1991).
[11] N. Ishimatsu, H. Hashizume, S. Hamada, N. Hosoito, C. S. Nelson, C. T. Venkataraman, G. Srajer, and J. C. Lang, Phys. Rev. B **60**, 9596 (1999).
[12] Y. Choi, D. Haskel, R. E. Camley, D. R. Lee, J. C. Lang, G. Srajer, J. S. Jiang, and S. D. Bader, Phys. Rev. B **70**, 134420 (2004).
[13] D. Haskel, G. Srajer, J. C. Lang, J. Pollmann, C. S. Nelson, J. S. Jiang, and S. D. Bader, Phys. Rev. Lett. **87**, 207201 (2001).
[14] C. S. Nelson, G. Srajer, J. C. Lang, C. T. Venkataraman, S. K. Sinha, H. Hashizume, N. Ishimatsu, and N. Hosoito, Phys. Rev. B **60**, 12234 (1999).
[15] D. R. Lee, S. K. Sinha, C. S. Nelson, J. C. Lang, C. T. Venkataraman, G. Srajer, and R. M. Osgood, Phys. Rev. B **68**, 224410 (2003).
[16] D. R. Lee, Y. J. Park, D. Kim, Y. H. Jeong, and K.-B. Lee, Phys. Rev. B **57**, 8786 (1998).
[17] J. S. Jiang and C. L. Chien, J. Appl. Phys. **79**, 5615 (1996).
[18] J. V. Harkins and P. Donovan, J. Magn. Magn. Mater. **156**, 224 (1996).
[19] P. Pankowski, L. T. Baczewski, T. Story, A. Wawro, K. Mergia, and S. Messoloras, Phys. Status Solidi C **1**, 405 (2004).
[20] K. Mergia, L. T. Baczewski, S. Messoloras, S. Hamada, T. Shinjo, H. Gamari-Seale, and J. Hauschild, Appl. Phys. A: Mater. Sci. Process. **74**, s1520 (2002).
[21] K. T. Moore and G. van der Laan, Rev. Mod. Phys. **81**, 235 (2009).
[22] R. Springell, S. W. Zochowski, R. C. C. Ward, M. R. Wells, S. D. Brown, L. Bouchenoire, F. Wilhelm, S. Langridge, W. G. Stirling, and G. H. Lander, J. Phys.: Condens. Matter **20**, 215229 (2008).
[23] R. Springell, S. W. Zochowski, R. C. C. Ward, M. R. Wells, S. D. Brown, L. Bouchenoire, F. Wilhelm, S. Langridge, W. G. Stirling, and G. H. Lander, J. Phys.: Condens. Matter **20**, 215230 (2008).
[24] R. Springell, F. Wilhelm, A. Rogalev, W. G. Stirling, R. C. C. Ward, M. R. Wells, S. Langridge, S. W. Zochowski, and G. H. Lander, Phys. Rev. B **77**, 064423 (2008).
[25] R. Springell, B. Detlefs, G. H. Lander, R. C. C. Ward, R. A. Cowley, N. Ling, W. Goetze, R. Ahuja, W. Luo, and B. Johansson, Phys. Rev. B **78**, 193403 (2008).
[26] L. T. Baczewski, P. Pankowski, A. Wawro, K. Mergia, S. Messoloras, and F. Ott, Phys. Rev. B **74**, 075417 (2006).
[27] C. F. Majkrzak, J. W. Cable, J. Kwo, M. Hong, D. B. McWhan, Y. Yafet, J. V. Waszczak, and C. Vettier, Phys. Rev. Lett. **56**, 2700 (1986).
[28] K. T. Moore, J. M. Howe, D. R. Veblen, T. M. Murray, and E. A. Stach, Ultramicroscopy **80**, 221 (1999).
[29] K. T. Moore, W. C. Johnson, J. M. Howe, H. I. Aaronson, and D. R. Veblen, Acta Mater. **50**, 943 (2002).
[30] M. Björck and G. Andersson, J. Appl. Crystallogr. **40**, 1174 (2007).
[31] L. G. Parratt, Phys. Rev. **95**, 359 (1954).
[32] L. Névot and P. Croce, Rev. Phys. Appl. **15**, 761 (1980).
[33] M. Tolan, W. Press, F. Brinkop, and J. P. Kotthaus, Phys. Rev. B **51**, 2239 (1995).
[34] S. K. Sinha, E. B. Sirota, S. Garoff, and H. B. Stanley, Phys. Rev. B **38**, 2297 (1988).
[35] V. Holý, J. Kuběna, I. Ohlídal, K. Lischka, and W. Plotz, Phys. Rev. B **47**, 15896 (1993).
[36] J.-P. Schlomka, M. Tolan, L. Schwalowsky, O. H. Seeck, J. Stettner, and W. Press, Phys. Rev. B **51**, 2311 (1995).
[37] E. Spiller, D. Stearns, and M. Krumrey, J. Appl. Phys. **74**, 107 (1993).
[38] V. M. Kaganer, S. A. Stepanov, and R. Köhler, Phys. Rev. B **52**, 16369 (1995).
[39] J. Daillant and O. Bélorgey, J. Chem. Phys. **97**, 5824 (1992).
[40] D. K. G. De Boer, A. J. G. Leenaers, and R. M. Wolf, J. Phys. D **28**, A227 (1995).
[41] D. E. Savage, J. Kleiner, Y.-H. Phang, T. Jankowski, J. Jacobs, R. Kariotis, and M. G. Lagally, J. Appl. Phys. **69**, 1411 (1991).
[42] J. Stettner, L. Schwalowsky, O. H. Seeck, M. Tolan, W. Press, C. Schwarz, and H. v. Kanel, Phys. Rev. B **53**, 1398 (1996).
[43] E. A. Kondrashkina, S. A. Stepanov, R. Opitz, M. Schmidbauer, R. Kohler, R. Hey, M. Wassermeier, and D. V. Novikov, Phys. Rev. B **56**, 10469 (1997).
[44] I. Pape, T. Hase, B. Tanner, and M. Wormington, Physica B **253**, 278 (1998).
[45] V. Holý, A. A. Darhuber, J. Stangl, G. Bauer, J. Nützel, and G. Abstreiter, Semicond. Sci. Technol. **13**, 590 (1998).
[46] Z. H. Ming, A. Krol, Y. L. Soo, Y. H. Kao, J. S. Park, and K. L. Wang, Phys. Rev. B **47**, 16373 (1993).
[47] R. S. Sayles and T. R. Thomas, Nature (London) **271**, 431 (1978).
[48] B. B. Mandelbrot, Science **156**, 636 (1967).
[49] M. V. Berry, J. Phys. A **12**, 781 (1979).
[50] C. Y. Poon, R. S. Sayles, and T. A. Jones, J. Phys. D **25**, 1269 (1992).
[51] G. P. Felcher, Phys. Rev. B **24**, 1595 (1981).
[52] S. Langridge *et al.*, Phys. Rev. B **74**, 014417 (2006).
[53] S. Langridge, J. Schmalian, C. H. Marrows, D. T. Dekadjevi, and B. J. Hickey, Phys. Rev. Lett. **85**, 4964 (2000).
[54] R. M. Osgood, III, S. K. Sinha, J. W. Freeland, Y. U. Idzerda, and S. D. Bader, J. Magn. Magn. Mater. **198-199**, 698 (1999).
[55] G. Beutier, G. van der Laan, K. Chesnel, A. Marty, M. Belakhovsky, S. P. Collins, E. Dudzik, J.-C. Toussaint, and B. Gilles, Phys. Rev. B **71**, 184436 (2005).
[56] J. F. MacKay, C. Teichert, D. E. Savage, and M. G. Lagally, Phys. Rev. Lett. **77**, 3925 (1996).

[57] J. M. Tonnerre, L. Sève, D. Raoux, G. Soullié, B. Rodmacq, and P. Wolfers, Phys. Rev. Lett. **75**, 740 (1995).
[58] F. de Bergevin, M. Brunel, R. M. Galéra, C. Vettier, E. Elkaim, M. Bessière, and S. Lefèbvre, Phys. Rev. B **46**, 10772 (1992).
[59] A. M. Beesley, S. W. Zochowski, M. F. Thomas, A. D. F. Herring, S. Langridge, S. D. Brown, R. C. C. Ward, M. R. Wells, R. Springell, and W. G. Stirling, J. Phys.: Condens. Matter **16**, 8507 (2004).
[60] S. D. Brown *et al.*, Phys. Rev. B **77**, 014427 (2008).
[61] M. F. Thomas, A. M. Beesley, R. C. C. Ward, and M. R. Wells, J. Phys.: Condens. Matter **20**, 365204 (2008).
[62] J. W. Freeland, K. Bussmann, Y. U. Idzerda, and C.-C. Kao, Phys. Rev. B **60**, R9923 (1999).